PHASE IMAGING: UNWRAPPING AND DENOISING WITH DIVERSITY AND MULTI-RESOLUTION

Gonçalo Valadão and José Bioucas-Dias

Instituto de Telecomunicações and Instituto Superior Técnico,
Av. Rovisco Pais, Torre Norte, Piso 10, 1049-001 Lisboa, Portugal
$email : \{gvaladao, bioucas\}@lx.it.pt$

ABSTRACT

Many imaging techniques, *e.g.*, interferometric synthetic aperture radar (InSAR), and magnetic resonance imaging (MRI), yield phase images. In these, generally, each pixel retrieves the phase up to a modulo-2π rad ambiguity, *i.e.*, the phase wrapped around the principal interval $[-\pi\ \pi[$. Phase unwrapping (PU) is, then, a crucial operation to obtain absolute phase, which is where physical information relies on. If the phase difference between neighbor pixels is less than π rad, then, phase unwrapping can be obtained unambiguously. This, however, is not always the case. *E.g.*, in InSAR, where absolute phase is proportional to terrain altitude, we often face neighbor phase differences much larger than π rad. The PU problem is even more challenging for noisy images. This paper proposes a diversity approach, which consists of using two (or more) images of the same scene acquired with different frequencies. Diversity grants an enlargement of the ambiguity interval $[-\pi\ \pi[$, thus, allowing to unwrap images with higher phase rates. Furthermore, this paper presents a multi-resolution technique to make denoising. We formulate the problem with a *maximum a posteriori* - Markov random field (MAP-MRF) rationale, and apply energy minimization techniques based on graph cuts. We illustrate the performance of the algorithm by showing experimental results, and argue that it is, as far as we know, state-of-the art.

1. INTRODUCTION

There are nowadays many applications based on phase images, *e.g.*, interferometric synthetic aperture radar (InSAR) [4], magnetic resonance imaging (MRI) [5], adaptive optics [6], vibration and deformation measurements [7], and diffraction tomography [8]. InSAR is being successfully applied, *e.g.*, to the generation of digital elevation models (DEM), and in the monitoring of land subsidence; among the many MRI applications, we emphasize venography (angiography as well) [9] and tissues elastography [10]; concerning adaptive optics, we point up applications in medicine and industry [11]; interferometry based vibration and deformation measurements is widespread among metrology techniques; diffraction tomography finds application in, *e.g.*, geophysical subsurface prospection and 3D microscopic imaging. In all of these imaging systems, the acquisition sensors read only the cosine and the sine components of the absolute phase; that is, we have access only to the phase modulo-2π, the so-called interferogram. Besides the sinusoidal nonlinearity, the observed data is corrupted by some type of noise. Due to these degradation mechanisms, phase unwrapping is known to be a very difficult problem. In fact, if the magnitude of phase variation between neighbor pixels is larger than π, *i.e.*, the so-called Itoh condition [12] is violated, then the inference of the 2π multiples is an ill-posed problem [13]. These violations may be due to undersampling, discontinuities, or noise.

1.1. Contributions

The main contribution of this paper is to present an algorithm that accomplishes both phase unwrapping and denoising.

Our approach is Bayesian. We adopt an observation model that is 2π-periodic, and discontinuity preserving MRF priors for the absolute phase. A MAP criterion infers the phase by exploiting graph-cuts based energy minimization techniques. The algorithm has two main steps:

1. Phase unwrapping: we input two (or more) different frequency interferograms (of the same scene), which provides an extension of the $[-\pi\ \pi[$ ambiguity interval and, consequently, an increasing of the phase rates that still allow unwrapping to be a well-posed problem. This frequency *diversity* technique is put forward through a graph-cuts algorithm [14] that minimizes a MRF composed of a sinusoidal data term plus a non-isotropic total variation (TV) prior [14].

2. Denoising: we achieve denoising by an iterative *multi-resolution* MAP-MRF energy minimization graph-cuts algorithm [15]. As in the previous step, (Phase unwrapping), the data term is sinusoidal, while a discontinuity preserving denoising prior is considered [15], [3].

This work was supported by the Instituto de Telecomunicações under the project IT/LA/325/2005.

We acknowledge Vladimir Kolmogorov for making public his max-flow optimization code [1].

This paper is based on previous technical reports [2] and [3].

1.2. Related work

Frequency diversity based PU algorithms are scarce. We are aware only of [16], [17], and [18] published in 1994, 1998 and 2002, respectively. Regarding the first [16] it proposes three very simple (and interesting) algorithms that, nonetheless, are error prone. With respect to the second [17], it is a multidimensional (accounting for multi-frequency) version of the minimum L^2 norm type of PU algorithm [19], with relaxation to the continuum that is well-known [19] to give rise to solving a Poisson equation. The weaknesses of this approach are long-familiar, in particular the oversmoothing of high phase rate slopes and discontinuities, which is further amplified by the proposed previous low-pass filtering stage (see [20] for a deeper discussion on this problem). Concerning [18], it consists of an algorithm based on a maximum likelihood estimation technique, whose goal is to approximate the unknown (true) surface by means of local planes. The approach assures the uniqueness of the solution even accounting for high phase rate slopes or discontinuities. However, the global optimization required to compute the maximum likelihood, by suggestion of the authors, is to be achieved by simulated annealing, which is a (nowadays) too much slow optimization technique to tackle this problem, for which, *e.g.*, graph-cuts techniques are much more suited.

In the field of phase unwrapping, we refer to [19] and references therein. The $\mathbb{Z}$ step of $\mathbb{Z}\pi$M [20] and PUMA [15] are phase unwrapping state-of-the-art algorithms. Regarding the former the present work extends it by allowing a much wider family of MRF derived energies, which brings discontinuity preservation ability by using non convex pairwise interactions; with respect to the latter, the present work is also an extension by either taking account of data evidence and being capable of denoising. We refer also the work in [21], from which we specially mention the unique denoising performance.

With respect to the optimizations, we deal with multi-labeling problems on energy (objective) functions having unary (one variable, data dependence) and binary (two variables, prior dependence) terms. Regarding this kind of problems, we highlight the algorithms proposed in [22], [23], [24], [25] and references therein; we note that although the expansion moves algorithm [22] is particularly successful in several applications, we found out not to be in ours. Regarding binary-labeling problems, we point out [26], [27], and references there presented.

2. PROPOSED FORMULATION

Let us consider the undirected graph $(\mathcal{V}, \mathcal{E})$ where the set of nodes $\mathcal{V}$ represents image pixels and the set of edges $\mathcal{E}$ represents pairs of neighboring pixels (horizontal and vertical in our case).

2.1. Posterior density

We consider, as in, *e.g.*, [20], the observation data model to be given by (1)

$$z = e^{jF\phi} + n, \tag{1}$$

where F is a constant to which we attach the meaning of frequency, ϕ is the absolute phase, and n a zero-mean, circular, Gaussian noise. Again we refer to [20] to state that the log-likelihood of the absolute phase, ϕ, given the observed wrapped phase, $\psi = \mathrm{angle(z)}$, is, then, given by (2)

$$f(\phi|\psi) = -\lambda \cos(\psi - F\phi) + c, \tag{2}$$

where $\lambda \propto |z|$, and c is an irrelevant constant. In what follows we can take $\lambda = 1$ without loss of generality. Considering also that the prior is a MRF, then the logarithm of the posterior density is given by (3)

$$E(\phi) \equiv \underbrace{\sum_{i \in \mathcal{V}} -\cos(\psi_i - F\phi_i)}_{\text{Data fidelity term}} + \mu \underbrace{\sum_{(i,j) \in \mathcal{E}} V(\phi_i, \phi_j)}_{\text{Prior term}}, \tag{3}$$

where $\phi = (\phi_1, \phi_2, \ldots, \phi_{|\mathcal{V}|})$, $\psi = (\psi_1, \psi_2, \ldots, \psi_{|\mathcal{V}|})$, V is a, to be specified, potential and finally, μ is the prior parameter that sets the relative weight between the data fidelity and the prior terms. We will now, in next section, detain on the data fidelity term of (3), and succintly introduce the frequency diversity notion.

2.2. Diversity

Several signal and image processing techniques employ diversity, which consists of signaling some event or target, *e.g.*, imaging an object, by using diverse relevant parameters. In this paper we consider frequency diversity which is particularly used in various areas, such as, *e.g.*, MRI, echographic Doppler, weather radar, and InSAR.

Namely, we deal with two (for the sake of simplicity) frequencies $F_1 = p/q$, $F_2 = r/s$ where $\{p, q, r, s\} \in \mathbb{N}$[1]. Assuming that observations (1) are independent for each frequency, the log-likelihood is given by (4)

$$f(\phi|\psi_1, \psi_2) = -\cos(\psi_1 - F_1\phi) - \cos(\psi_2 - F_2\phi), \tag{4}$$

We have already alluded (Section 1.1) to the advantage that frequency diversity gives in extending the $[-\pi\ \ \pi[$ ambiguity interval. Stating it more clearly, it is easy to show that the sum of two cosine functions, having as in (4) different frequencies $F_1 = p/q$ and $F_2 = r/s$, where $\{p, q\}, \{p, r\}, \{q, s\}$, and $\{r, s\}$ are coprime integers[2], results in a third periodic function whose period is $q \times s$; as the initial functions do have periods of respectively q and s, we conclude that the period is, in general, extended and so the ambiguity reduced. Fig.1 illustrates this effect by plotting the function $f(t) = \cos(t) + \cos(2/5\ t),\ t \in [-8\ \ 8]$ with t in 2π rad units. It can be seen that the period has been extended five times (the initial periods were 2π rad and $5 \times 2\pi$ rad). This "beat production", well known in wave physics, can also be understood by the Chinese remainder theorem [28].

[1] Rigorously, F_1 and F_2 can be irrational as long as their quotient is rational. However this does not make any loss of generality in what follows.

[2] Two integer numbers are said to be coprime if their greatest common divisor is the unity.

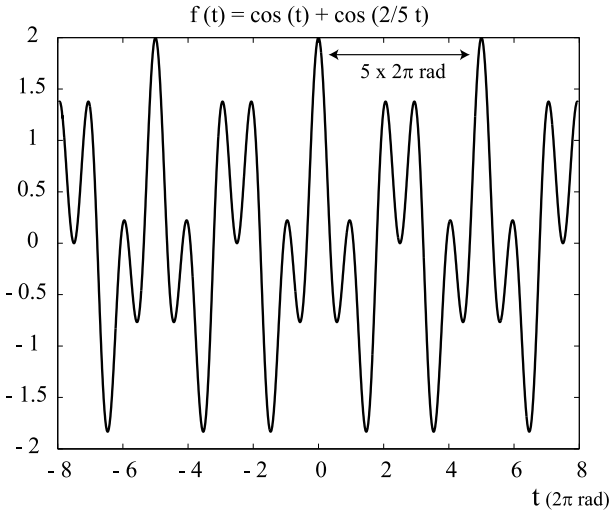

Figure 1. Ambiguity reduction by summing two periodic functions: the beat effect.

It is a well known behavior, *e.g.*, from wave phenomena, that the greater the beat period extension, the smaller the difference between global and local maxima. Furthermore, it is also well known that beat period extension brings noise amplification. This trade-off should then be taken into account.

2.3. Phase unwrapping with diversity

Replacing the data fidelity term in (3) with that given by (4), *i.e.*, considering diversity, we obtain

$$E(\phi) \equiv \sum_{i\in\nu} -\cos\left(\psi_{1_i} - F_1\phi_i\right) - \cos\left(\psi_{2_i} - F_2\phi_i\right) + \mu \sum_{(i,j)\in\mathcal{E}} V\left(\phi_i, \phi_j\right), \quad (5)$$

where $\phi = (\phi_1, \phi_2, \ldots, \phi_{|\mathcal{V}|})$, $\psi_1 = (\psi_{1_1}, \psi_{1_2}, \ldots, \psi_{1_{|\mathcal{V}|}})$, $\psi_2 = (\psi_{2_1}, \psi_{2_2}, \ldots, \psi_{2_{|\mathcal{V}|}})$, V is the prior potential, and, finally, μ is the regularization parameter that sets the relative weight between the data fidelity and the prior terms.

In this section we solve only the phase unwrapping problem. So, by admitting a noiseless environment, we may consider that the unwrapped (true) phase ϕ is given by:

$$F_1\phi = \psi_1 + 2k_1\pi, \quad (6)$$

and

$$F_2\phi = \psi_2 + 2k_2\pi, \quad (7)$$

for the two independent observations with frequencies F_1 and F_2, respectively. For the sake of simplicity we can deal with (6) only, and (5) turns[3] into:

$$E(k) \equiv \sum_{i\in\mathcal{V}} -\cos\left(\psi_{2_i} - \frac{F_2}{F_1}(\psi_{1_i} - 2k_{1_i}\pi)\right) + \mu \sum_{(i,j)\in\mathcal{E}} V\left(\psi_{1_i} - 2k_{1_i}, \psi_{1_j} - 2k_{1_j}\right), \quad (8)$$

[3]We could have dealt with both observations simultaneously. For simplicity we do not.

with a correspondingly combinatorial optimization (minimization) to be done on variables k_{1_i}.

We take $V\left(\psi_{1_i} - 2k_{1_i}, \psi_{1_j} - 2k_{1_j}\right) = |k_i - k_j|$ the, so-called, non-isotropic TV; in spite of such a potential being convex, which confers some optimization "easiness" (see, *e.g.*, [29] for a nice view on this "easiness" on combinatorial optimization problems), it still has some discontinuity preservability properties.

We are aware of only three integer optimization algorithms, that are able to provide a global minimum for a posterior energy like (8), which is composed by a non-convex data fidelity term and a convex prior potential. Those algorithms were introduced in [30], [31], and [14]. Herein we refer to the last one [14], as it deals with our non-isotropic TV prior. As long as the energy is a levelable function, i.e., a function that admits a decomposition as a sum on levels, of functions of its variables level-set indicatrices at current level (see [14]), it is easy to build a source-sink graph such that its maxflow is the sought global minimum. For the sake of simplicity we do not describe the above mentioned energy decomposition on level-set dependent functions, as we will not describe in detail the graph construction. In Fig. 2 (very similar to the one presented in [14]) we represent a graph corresponding to a toy example of an image with 3 pixels and 3 available labels (k_i values in our case). The source and the sink are respectively denoted by s and t. We note that all nodes are connected to the source s and to the sink t for although all arcs are not depicted. In our experimental results we have used the augmenting path type maxflow/min-cut algorithm proposed in [1]. The worst case complexity for augmenting path algorithms is $O(n^2m)$ [32], where n and m are the number of vertices and edges, respectively. However, in a huge array of experiments conducted in [1], authors systematically found out a complexity that is inferior to that of the push-relabel algorithm [33], with the queue based selection rule, which is $O(n\sqrt{m})$. Thus, we herein take this bound, which means a very low polynomial complexity maxflow algorithm. We remark, furthermore, that is simple to prove that non-isotropic TV is a levelable function.

2.4. Denoising with multi-resolution

For denoising we will take the potential (9) plotted in Fig.3

$$V(x) = \begin{cases} x^2, & |x| \leq \pi \\ \pi^{2-0.1}\,|x|^{0.1}, & |x| > \pi\,. \end{cases} \quad (9)$$

This potential is quadratic in an origin neighborhood of radius π in order to model Gaussian noise, and almost flat elsewhere to preserve discontinuities [34]. The radius of π is chosen because we expect to get (most of the) noise wrapped into the interval $[-\pi\ \pi[$ after the previous phase unwrapping step. Anyway, the concepts next introduced are still valid for a wide class of potential functions.

For the sake of clarity we refer back to the posterior density expression (3), which writes energy as $E \equiv E(\phi)$. Our goal is to compute $\phi^* = \arg\min\left[E(\phi)\right]$. We note

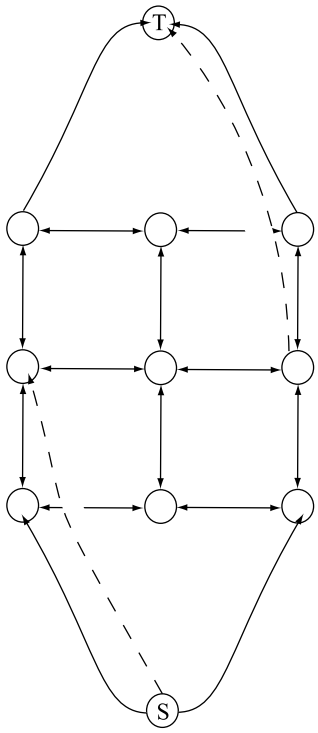

Figure 2. Sketch of the graph used to perform phase unwrapping. Toy example.

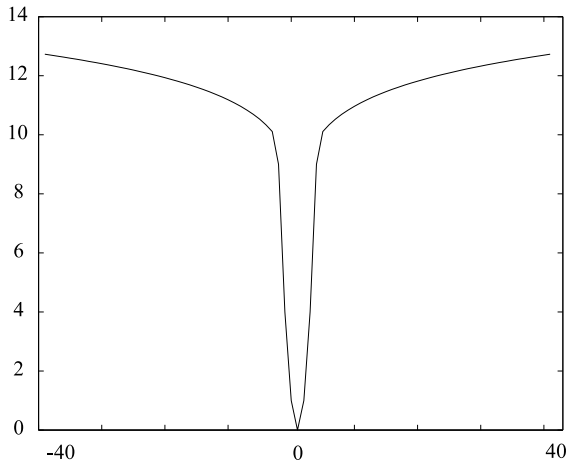

Figure 3. Plot of the function whose analytical expression is given by (9).

that the objective function, $E(\phi)$, is non-convex (both in the data fidelity term and in the prior term), which makes this optimization problem very difficult. Instead of solving this problem in $\mathbb{R}^{|\mathcal{V}|}$, we discretize the domain of E, using a discretization interval Δ. In doing this, we converted the minimization in $\mathbb{R}^{|\mathcal{V}|}$ into a labeling (*i.e.*, combinatorial) problem that, under given conditions, may be solved efficiently by computing flows on graphs. Furthermore, we have chosen to make the denoising optimization, using one frequency data only. We decided to perform this way because by using the two frequencies the objective function got a huge amount of local minima and, accordingly, the problem got intractable. In doing this we are already deciding for a sub-optimal solution.

A minimization on the discrete domain yielding a minimizer close to the one obtained in the $\mathbb{R}^{|\mathcal{V}|}$, suggests a "small" discretization interval. On the other hand, small values of Δ leads to huge configuration spaces and associated computation burdens; furthermore it may favor the probability of getting stuck in local minima. We circumvent this by adopting a multi-resolution strategy in which the minimum of E is searched for in a sequence of increasing resolutions. To this end, let us define $\delta_i \in \{0, 1\}$, for $i \in \mathcal{V}$, and the sets

$$\begin{aligned} \mathcal{M}^U(\phi', \Delta) &\equiv \{\phi_i,\, i \in \mathcal{V} : \phi_i = \phi'_i + \delta_i \Delta\} \\ \mathcal{M}^D(\phi', \Delta) &\equiv \{\phi_i,\, i \in \mathcal{V} : \phi_i = \phi'_i - \delta_i \Delta\} \end{aligned}$$

Algorithm 1 shows the pseudo-code for our optimization scheme ($\phi = \{\phi_i\}$); we emphasize that $E(\phi)$ is a function of the potential V according to (8).

Algorithm 1 Denoising with multi-resolution.

Require: $\phi = \psi$ {Interferogram}, successup = false, successdown = false

for $\Delta = 2\pi \times \left\{2^0, 2^{-1}, \ldots, 2^{-N}\right\}$ **do**
  while (successup = false OR successdown = false) **do**
    if successup = false **then**
      $\hat{\phi} = \arg\min_{\phi \in M^U(\phi, \Delta)} E(\phi)$
      if $E(\hat{\phi}) < E(\phi)$ **then**
        $\phi = \hat{\phi}$
      else
        successup = true
      end if
    end if
    if successdown = false **then**
      $\hat{\phi} = \arg\min_{\phi \in M^D(\phi, \Delta)} E(\phi)$
      if $E(\hat{\phi}) < E(\phi)$ **then**
        $\phi = \hat{\phi}$
      else
        successdown = true
      end if
    end if
  end while
end for

Our algorithm engages on a greedy succession of up and down binary optimizations. The precision of the minimization, Δ, starts with the value 2π and ends with the value $2\pi/(2^N)$ where N is a depth of resolution. We point out that even if all the computations could have been done with the highest Δ resolution level[4] from the very beginning, choosing this multi-resolution schedule increases dramatically (a logarithmic improvement) the algorithm speed.

To solve the binary optimizations shown in lines 4 and 12 of Algorithm 1, we use the graph-cuts technique presented in [29]. For the sake of simplicity we will not repeat here the graph construction, which is in the referred work clearly presented, on which we compute the min-cut (which is equal to max-flow as stated by Ford-Fulkerson Theorem [35]) to obtain the desired optimization. We further add that we have adopted a MM [36] technique identical to the one we have applied in [15], to deal with non-convex potentials, non-convexity giving rise to non-regularity [29].

We should note that we do not have any guarantees of reaching a global minimum with Algorithm 1. This is so because, with generality, we are dealing with both non-convex data fidelity terms and prior terms. However, experimental results in a series of experiments on simulated and real data have been systematically state-of-the art.

3. PROPOSED ALGORITHM

The previous sections culminate in our phase imaging algorithm. It consists of a phase unwrapping stage and then denoising. Algorithm 2 shows a simple two lines high level pseudo-code of our phase imaging algorithm.

Algorithm 2 Phase imaging algorithm

1: Do phase unwrapping with diversity
2: Do denoising with multi-resolution

In the next section we show some relevant experimental results.

4. EXPERIMENTAL RESULTS

In this section, we briefly illustrate the performance of our algorithm on two representative phase unwrapping plus denoising problems.

Fig. 4 (a) displays an image, 100×150 pixels, which can be described as a sheared ramp whose maximum height is 99 rad. Figs. 4 (b) and (c) show the corresponding wrapped images (black corresponds to $-\pi$ and white to π), having Gaussian noise with standard deviation $\sigma = 0.3162$ rad corresponding to signal to noise ratio SNR=10 dB. Each one of the wrapped images is acquired with two frequencies of, respectively, $F_1 = 1/1$ and $F_2 = 7/8$. Fig. 4 (d) displays an image of the unwrapped sheared ramp, and Fig. 4 (e) shows a corresponding 3-D rendering. Fig. 4 (f) shows a 3-D rendering after the denoising step. It is quite clear that our algorithm had a very good performance at both phase unwrapping (perfect) and denoising. We stress that the discontinuity created by the shear and the noise allied to the inclination angle of the ramp, poses a hard PU problem because several phase jumps of magnitude greater than π arise[5]. The diversity information plus the discontinuity preserving potential play a crucial role in the good performance. Figs. 4 (g) and (h) show the histograms (the axis are in rad) corresponding to the surfaces rendered in Figs. 4 (e) and (f), respectively. It is evident the denoising accomplishment. The first row of table 1 presents the corresponding standard deviations (in rad) of the error relative to the original image [Fig.4 (a)] as well as the related improvement in signal to noise ratio (ISNR). Still referring to the histograms, the one corresponding to the noise image shows a multi modal shape. Besides the central mode around zero, there are two modes around -2π and 2π respectively. Those correspond to "spikes" as a result of the data observation model. After denoising they do disappear.

Fig. 5 (a) displays an image, 100×100 pixels, which is given by a Gaussian having maximum height of 50π rad height, and standard deviations of 10 pixels (horizontal) and 15 pixels (vertical). Figs. 5 (b) and (c) show the corresponding wrapped images (black corresponds to $-\pi$ and white to π), having a Gaussian noise with standard deviation $\sigma = 0.3162$ rad corresponding to SNR $= 10$ dB. Each one of the wrapped images is acquired with two frequencies of, respectively, $F_1 = 1/1$ and $F_2 = 7/8$. Fig. 5 (d) displays an image of the unwrapped sheared ramp, and Fig. 5 (e) shows a corresponding 3-D rendering. Fig. 5 (f) shows a 3-D rendering after the denoising step. It is quite clear that our algorithm had an excellent performance at phase unwrapping. We stress that the high phase rates of the Gaussian *per se* poses a hard PU problem because many phase jumps of magnitude greater than π arise. This may be observed in the aliasing effects that appear in Figs. 5 (b) and (c). The noise enlarges this "jumps effect". The diversity information is crucial to the perfect phase unwrapping (with one source only, it is an impossible task). Concerning the denoising step, the performance is far from perfect. Even so, we can realize that some denoising has occurred, since the surface becomes smoother. However there are quite a lot of craters in the surface. This, far from perfect, denoising is reflected in Figs. 5 (h) and (i), which show the histograms (the axis are in rad) corresponding to the surfaces rendered in Figs. 5 (e) and (f), respectively. Also the second row of table 1 presents the corresponding standard deviations (in rad) of the error relative to the original image [Fig. 5 (a)], as well as the related improvement in signal to noise ratio (ISNR). In fact the prior that we have employed models images that are region-wise-smooth, so this behavior was expected. The approach presented in [21] is much more suitable in this case. We tried to improve the performance on the noisy image in Fig. 5 (e). For that we simply ap-

[4] As already mentioned above, it is not a good idea to start with the highest (finest) resolution, because that improves the possibility of getting stuck on local minima

[5] Even if the ramp inclination by itself, (not considering the shear), does not generate, greater than π, in magnitude, jumps.

plied a median filter (3×3 kernel). The resulting image is rendered in Fig. 5 (g), whose corresponding histogram is shown in 5 (h). It is evident (specially in the histogram) that the median filter works better, in this very difficult case, than our proposed denoising step. The standard deviation of the median filtered image is 0.5201 rad which confirms the visual inspection. Still referring to the histograms, the one corresponding to the noise image shows a multi modal shape. Besides the central mode around zero, there are two modes around -2π and 2π respectively. Those correspond to "spikes" as a result of the data observation model. After denoising they do disappear, although some new ones, more near to the origin, do appear. After median filtering denoising, there remains only one mode around the origin.

Table 1. Phase imaging performance.

	std noisy (rad)	std denoised (rad)	ISNR (dB)
Ramp	0.6542	0.2136	7.9
Gaussian	1.0114	0.8938	0.3756

5. CONCLUDING REMARKS

We have proposed a phase imaging algorithm, that makes phase unwrapping with diversity and denoising with multi-resolution. Our approach is a MAP-MRF one. We have chosen both non-convex data fidelity and prior potential terms, in the MAP-MRF, so there is no hope to find the global minimum efficiently. Thus, we propose a sub-optimal minimization based on graph cuts. Our approach inherits much of our previous work, PUMA [15], however we do have extended it, by taking into account a data fidelity term and denoising. This fact, plus very good results, leads us to argue that our approach is state-of-the-art (as far as we are aware). In the second experimental result, Fig. 5, we have illustrated some difficulty in achieving proper denoising. In particular, the multi-modal histogram in Fig. 5 (i), stirs us to refine our noise model in the future, by using, *e.g.*, a Gaussian mixture rationale.

6. REFERENCES

[1] Y. Boykov and V. Kolmogorov, "An experimental comparison of min-cut/max-flow algorithms for energy minimization in vision," *IEEE Transactions on Pattern Analysis and Machine Intelligence*, vol. 26, no. 9, pp. 1124–1137, 2004.

[2] J. Bioucas-Dias and G. Valadão, "Phase unwrapping via diversity and graph cuts," Tech. Rep., IT/IST Communications Theory and Pattern Recognition Group Report, Lisboa, Portugal, 2008.

[3] G. Valadão and J. Bioucas-Dias, "Discontinuity preserving absolute phase estimation: a multiprecision approach," Tech. Rep., IT/IST Communications Theory and Pattern Recognition Group Report, Lisboa, Portugal, 2008.

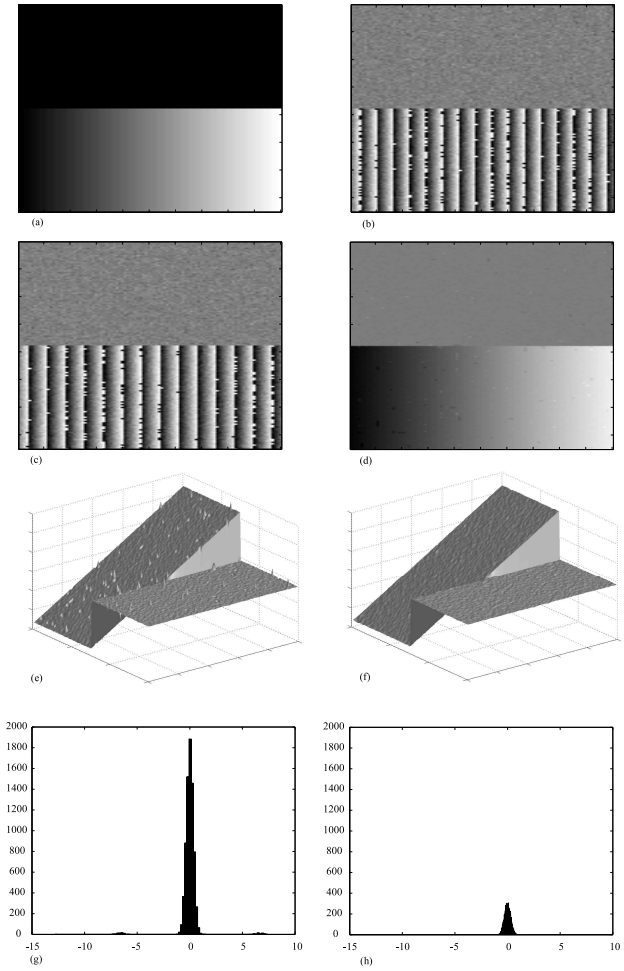

Figure 4. (a) Original sheared ramp phase image. (b) Image in (a) wrapped with a relative frequency of 1. (c) Image in (a) wrapped with a relative frequency of $7/8$. (d) Unwrapped image from the previous wrapped images shown in (b) and (c). (e) 3-D rendering of the image in (d). (f) 3-D rendering of the image in (d) after the denoising step. (g) Histogram corresponding to the surface rendered in (e). (h) Histogram corresponding to the surface rendered in (f).

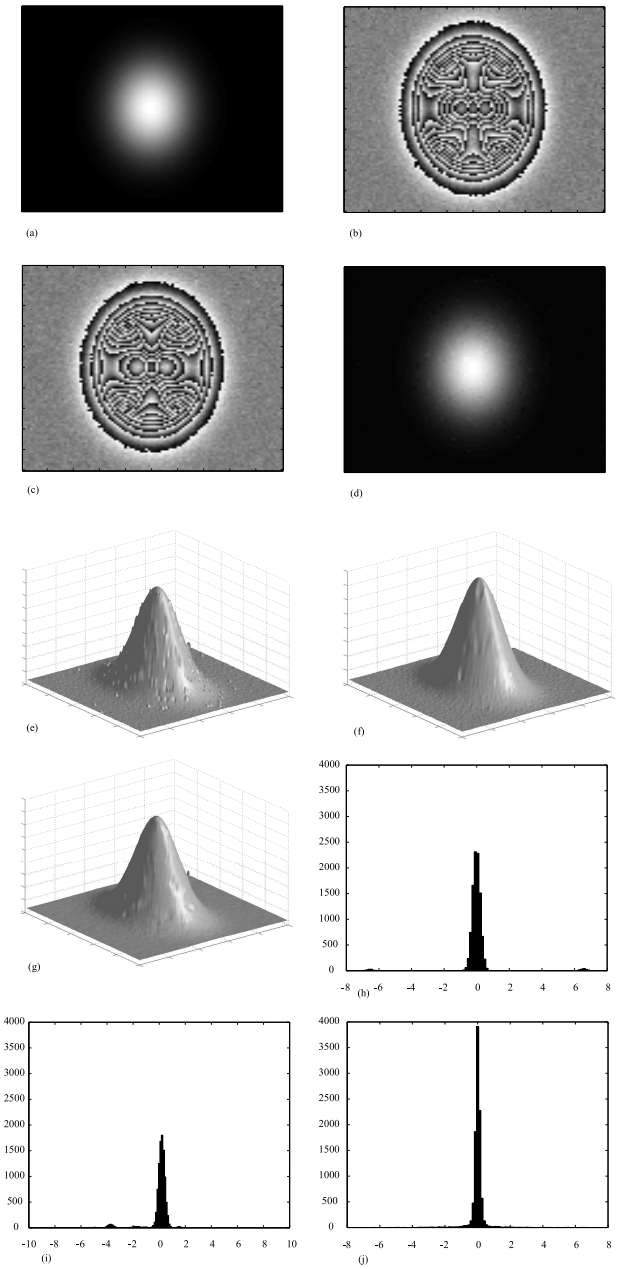

Figure 5. (a) Original Gaussian phase image. (b) Image in (a) wrapped with a relative frequency of 1. (c) Image in (a) wrapped with a relative frequency of $7/8$. (d) Unwrapped image from the previous wrapped images shown in (b) and (c). (e) 3-D rendering of the image in (d). (f) 3-D rendering of the image in (d) after the denoising step. (g) 3-D rendering of the image in (d) after the median filter denoising. (h) Histogram corresponding to the surface rendered in (e). (i) Histogram corresponding to the surface rendered in (f). Histogram corresponding to the surface rendered in (g).

[4] P. Rosen, S. Hensley, I. Joughin, F. LI, S. Madsen, E. Rodriguez, and R. Goldstein, "Synthetic aperture radar interferometry," *Proceedings of the IEEE*, vol. 88, no. 3, pp. 333–382, March 2000.

[5] P. Lauterbur, "Image formation by induced local interactions: examples employing nuclear magnetic resonance," *Nature*, vol. 242, pp. 190–191, March 1973.

[6] D. L. Fried, "Adaptive optics wave function reconstruction and phase unwrapping when branch points are present," *Optics Communications*, vol. 200, no. 1, pp. 43–72, December 2001.

[7] S. Pandit, N. Jordache, and G. Joshi, "Data-dependent systems methodology for noise-insensitive phase unwrapping in laser interferometric surface characterization," *Journal of the Optical Society of America*, vol. 11, no. 10, pp. 2584–2592, 1994.

[8] A. Devaney, "Diffraction tomographic reconstruction from intensity data," *IEEE Transactions on Image Processing*, vol. 1, pp. 221–228, April 1992.

[9] A. Rauscher, M. Barth, J. Reichenbach, R. Stollberger, and E. Moser, "Automated unwrapping of mr phase images applied to bold mr-venography at 3 tesla," *Journal of Magnetic Resonance Imaging*, vol. 18, no. 2, pp. 175–180, 2003.

[10] A. Manduca et al., "Magnetic resonance elastography: Non-invasive mapping of tissue elasticity," *Medical Image Analysis*, vol. 5, no. 4, pp. 237–254, December 2001.

[11] Michael C. Roggemann and Byron M. Welsh, *Imaging Through Turbulence*, CRC, 1996.

[12] K. Itoh, "Analysis of the phase unwrapping problem," *Applied Optics*, vol. 21, no. 14, 1982.

[13] J. Hadamard, "Sur les problèmes aux dérivées partielles et leur signification physique," *Princeton University Bulletin*, , no. 13, 1902.

[14] J. Darbon and M. Sigelle, "Image restoration with discrete constrained total variation part ii: Levelable functions, convex priors and non-convex cases fast and exact optimization," *Journal of Mathematical Imaging and Vision*, pp. 277–291, 2006.

[15] J. Bioucas-Dias and G. Valadão, "Phase unwrapping via graph cuts," *IEEE Transactions on Image Processing*, vol. 16, no. 3, pp. 698–709, March 2007.

[16] W. Xu, E. Chang, L. Kwoh, H. Lim, and W. Heng, "Phase-unwrapping of sar interferogram with multi-frequency or multi-baseline," in *Proceedings of the 1994 International Geoscience and Remote Sensing Symposium-IGARSS'94*, 1994, vol. 2, pp. 730–732.

[17] M. Vinogradov and I. Elizavetin, "Phase unwrapping method for the multifrequency and multibaseline interferometry," in *Proceedings of the 1998 International Geoscience and Remote Sensing Symposium-IGARSS'98*, Seattle, WA, USA, 1998, vol. 2, pp. 1103–1105.

[18] V. Pascazio and G. Schirinzi, "Multifrequency insar height reconstruction through maximum likelihood estimation of local planes parameters," *IEEE Transactions on Image Processing*, vol. 11, pp. 1478–1489, December 2002.

[19] D. Ghiglia and M. Pritt, *Two-Dimensional Phase Unwrapping. Theory, Algorithms, and Software*, John Wiley & Sons, New York, 1998.

[20] J. Dias and J. Leitão, "The $\mathbb{Z}\pi$M algorithm for interferometric image reconstruction in SAR/SAS," *IEEE Transactions on Image Processing*, vol. 11, pp. 408–422, April 2002.

[21] V. Katkovnik, J. Astola, and K. Egiazarian, "Noisy phase unwrap for fringe techniques: adaptive local polynomial approximations," in *Proceedings of the International Conference: True-Vision, Capture, Transmission, and Display of 3D Video (3DTV-CON 2007)*, 2007.

[22] Y. Boykov, O. Veksler, and R. Zabih, "Fast approximate energy minimization via graph cuts," *IEEE Transactions on Pattern Analysis and Machine Intelligence*, vol. 23, no. 11, pp. 1222–1239, 2001.

[23] V. Kolmogorov, "Primal-dual Algorithm for Convex Markov Random Fields," Tech. Rep., Microsoft Research Technical Report, Cambridge, 2005.

[24] J. Darbon, *Composants logiciels et algorithmes de minimisation exacte d'énergies dédiés au traitement des images*, Ph.D. thesis, Ecole Nationale Supérieure Des Télécommunications, 2005.

[25] J. Darbon, "Global Optimization for First Order Markov Random Fields with Submodular Priors," Tech. Rep., UCLA Computational and Applied Mathematics Report, Los Angeles, 2007.

[26] P. L. Hammer, P. Hansen, and B. Simeone, "Roof duality, complementation and persistency in quadratic 0-1 optimization," *Mathematical Programming*, vol. 28, pp. 121–155, 1984.

[27] C. Rother, V. Kolmogorov, V. Lempitsky, and M. Szummer, "Optimizing Binary MRFs via Extended Roof Duality," in *Proceedings of the IEEE Computer Society Conference on Computer Vision and Pattern Recognition*, 2007.

[28] K. Ireland and M. Rosen, *A Classical Introduction to Modern Number Theory, 2nd ed.*, Springer-Verlag.

[29] V. Kolmogorov and R. Zabih, "What energy functions can be minimized via graph cuts?," *IEEE Transactions on Pattern Analysis and Machine Intelligence*, vol. 26, no. 2, pp. 147–159, February 2004.

[30] H. Ishikawa, "Exact optimization for Markov random fields with convex priors," *IEEE Transactions on Pattern Analysis and Machine Intelligence*, vol. 25, no. 10, pp. 1333–1336, October 2003.

[31] Boris Zalesky, "Efficient determination of gibbs estimators with submodular energy functions," 2003.

[32] D. Bertsekas, *Network Optimization: Continuous and Discrete Models*, Athena-Scientific, 1998.

[33] A. Goldberg and R. Tarjan, "A new approach to the maximum-flow problem," *Journal of the Association for Computing Machinery*, vol. 35, no. 4, pp. 921–940, October 1988.

[34] S. Z. Li, *Markov Random Field Modeling in Computer Vision*, vol. 9 of *Computer Science Workbench*, Springer-Verlag, New York, 1995.

[35] L. Ford and D. Fulkerson, *Flows in Networks*, Princeton University Press, 1962.

[36] K. Lange, *Optimization*, Springer Verlag, New York, 2004.